ACS NANOSCIENCE Au
AN OPEN ACCESS JOURNAL OF THE AMERICAN CHEMICAL SOCIETY

pubs.acs.org/nanoau Article

Gold Nanoparticle Smartphone Platform for Diagnosing Urinary Tract Infections

Kyryl Zagorovsky,[▽] Maria Teresa Fernández-Argüelles,[▽] Diane Bona, Ashraf Mohamed Elshawadfy, Abdullah Muhammad Syed, Pranav Kadhiresan, Tony Mazzulli, Karen L. Maxwell, and Warren C.W. Chan*

Cite This: *ACS Nanosci. Au* 2022, 2, 324–332 Read Online

ACCESS | Metrics & More | Article Recommendations | Supporting Information

ABSTRACT: Current urinary tract infection (UTI) diagnostic methods are slow or provide limited information, resulting in prescribing antibiotic therapy before bacterial pathogen identification. Here, we adapted a gold nanoparticle colorimetric approach and developed a smartphone platform for UTI detection. We show the parallel identification of five major UTI pathogens at clinically relevant concentrations of 10^5 bacteria/mL using bacteria-specific and universal probes. We validated the diagnostic technology using 115 positive and 19 negative samples from patients with *Escherichia coli*, *Proteus mirabilis*, and *Klebsiella pneumoniae* infections. The assay successfully identified the infecting pathogen (specificity: >98% and sensitivity: 51−73%) in 3 h. Our platform is faster than culturing and can wirelessly store and transmit results at the cost of $0.38 per assay.

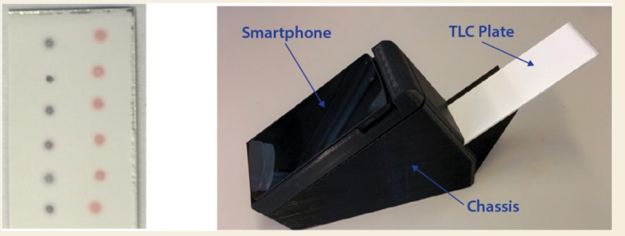

KEYWORDS: *diagnostics, urinary tract infection, gold nanoparticles, DNAzymes, smartphone, point of care device*

INTRODUCTION

Urinary tract infections (UTIs) are among the most common infections in children and affect more than 40% of women worldwide.[1,2] Major UTI bacterial pathogens include *Escherichia coli*, *Staphylococcus saprophyticus*, *Klebsiella pneumoniae*, *Enterococcus faecalis*, and *Proteus mirabilis*. Less frequently, *Pseudomonas aeruginosa*, *Enterobacter* spp., *Serratia* spp, *Citrobacter* spp., and *Candida albicans* are also found.[3−5] Clinicians perform UTI diagnosis by combining clinical history, physical examination, urinalysis, and bacterial culturing.[1] However, treatment based on the clinical history and physical examination leads to high false positives, while culturing suffers from assay times that can be as long as 48 h. Delay in the initiation of treatment can lead to a poorer therapeutic prognosis.[6,7] They generally prescribe initial treatment before the requirement for therapy has been verified, often leading to unnecessary antibiotic prescriptions. Urinalysis tests have low sensitivity or specificity and can only detect the presence of infection but cannot identify the specific pathogen, providing limited diagnostic information.[1]

There is a strong need to develop rapid diagnostic assays for UTIs to identify specific pathogens within hours rather than days. The availability of testing results early can improve patient outcomes, reduce the number of laboratory tests, and reduce invasive procedures and the length of hospital stays.[8−10] Since different organisms can cause UTIs, the platform must detect multiple pathogens in parallel. The diagnostic assay should also be suitable for point-of-care settings and be capable of sharing test results with a central computer system.[11] Decentralized testing combined with wireless communication would enable greater access to diagnostics, reduce the burden on the health care system, and facilitate infection tracking.[12] While polymerase chain reaction (PCR) tests are being adapted for UTI detection in laboratories, researchers have developed a lateral flow immunoassay for point-of-care test. The lateral flow immunoassay is simple to use and does not require extraction of samples; the adaption of this technique for multiplex testing and for detecting viral mutations that may lead to antimicrobial resistance is difficult.[12]

We recently reported a point-of-care assay that combines the signal amplification of a DNA-based multicomponent nucleic acid enzyme (Mz) with gold nanoparticles (GNPs). This approach can detect genetic targets via a colorimetric readout.[13−15] Here, we adapt this technology for the detection of UTI pathogens. We also develop a smartphone device capable of automating the analysis of the colorimetric signal from the GNP-Mz assay. The smartphone will be a critical feature for the automation of the assay and will allow electronic

Received: January 12, 2022
Revised: March 20, 2022
Accepted: March 21, 2022
Published: April 4, 2022

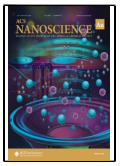

https://doi.org/10.1021/acsnanoscienceau.2c00001
ACS Nanosci. Au 2022, 2, 324−332

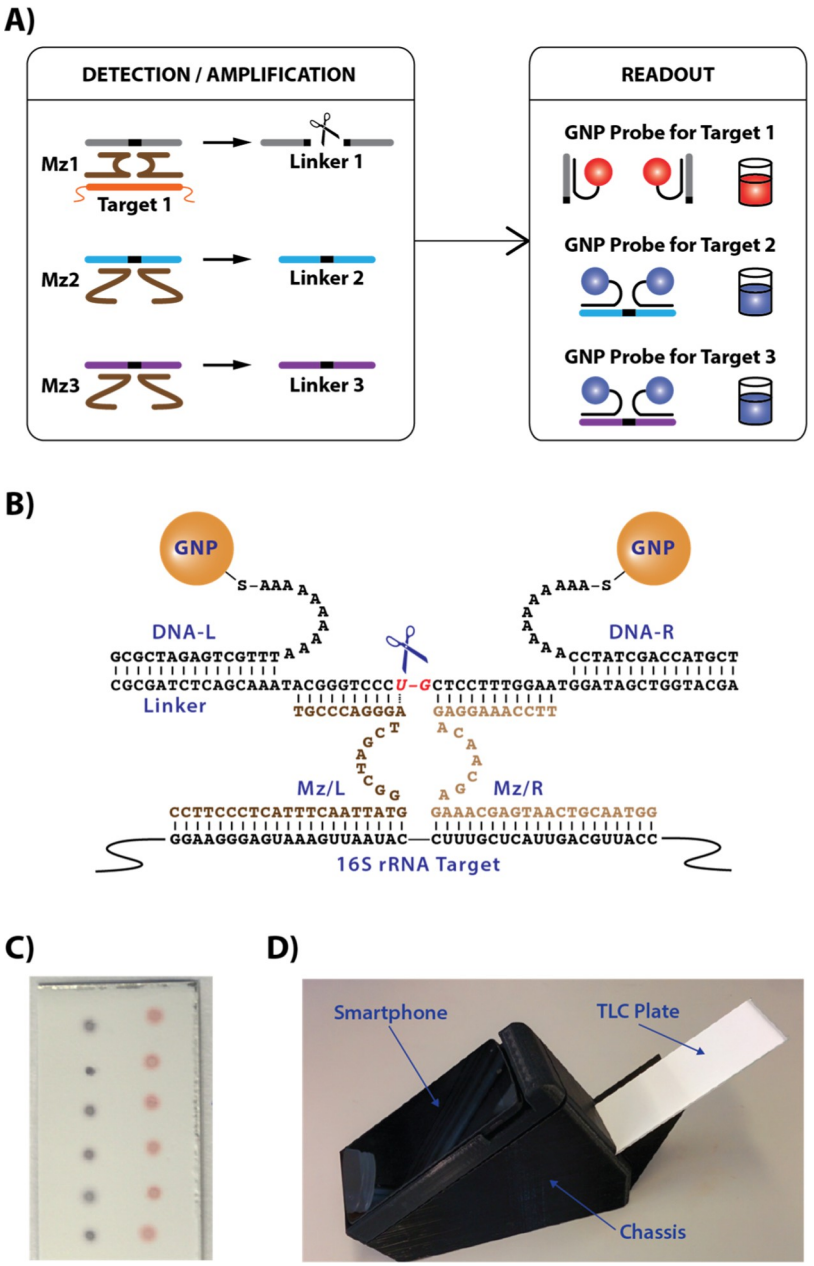

Figure 1. (A) Schematic of the overall assay. All Mz and linker components are mixed in a single test tube with the extracted patient sample. Target 1 activates Mz1 by cleaving linker 1, leading the separation of the GNP probe and a red solution color. Mz2 and Mz3 remain inactive, leading to a purple solution color from linkers 1 and 2 crosslinking the GNP probes. (B) Schematic showing the Mz catalytic complex. (C) Photograph of the spotted GNP probes on a TLC plate. Dark spots on the left represent negative results, and red spots on the right indicate positive detection. (D) Smartphone device designed for the TLC plate readout. The 3D-printed chassis includes LED lights for uniform plate illumination, batteries, and smartphone connection slots. A smartphone takes photographs of the TLC plate and transfers the resulting image to the server for image processing and spot color characterization.

storage of the test data and long-term geospatial tracking of infections.

RESULTS

Detection Scheme

We began by adapting our colorimetric diagnostic platform to detect bacterial targets based on their 16S rRNA signatures. Figure 1A shows the assay schematics. Two sets of 13 nm diameter GNPs were functionalized either with DNA strand DNA-L or strand DNA-R through thiol-gold coordinate bond formation.[16] We designed a linker DNA molecule to crosslink GNPs by hybridizing DNA-L and DNA-R strands. Nanoparticles absorbed strongly at 520 nm wavelength and appeared bright red due to the surface plasmon resonance (SPR) associated with the GNP surface. However, crosslinking by the linker DNA brought GNPs close together and caused SPR coupling of individual particles. As a result, the absorption wavelength red-shifted, and the GNP color changed from red to purple.[17] Linker DNA also included a sequence that could be bound and cleaved by the multicomponent nucleic acid enzyme Mz. Our Mz design was a modified version of the DNAzyme design from refs 18 and 19 for gene targeting.[20] Initially, binding the 16S rRNA target through hybridization

https://doi.org/10.1021/acsnanoscienceau.2c00001
ACS Nanosci. Au 2022, 2, 324−332

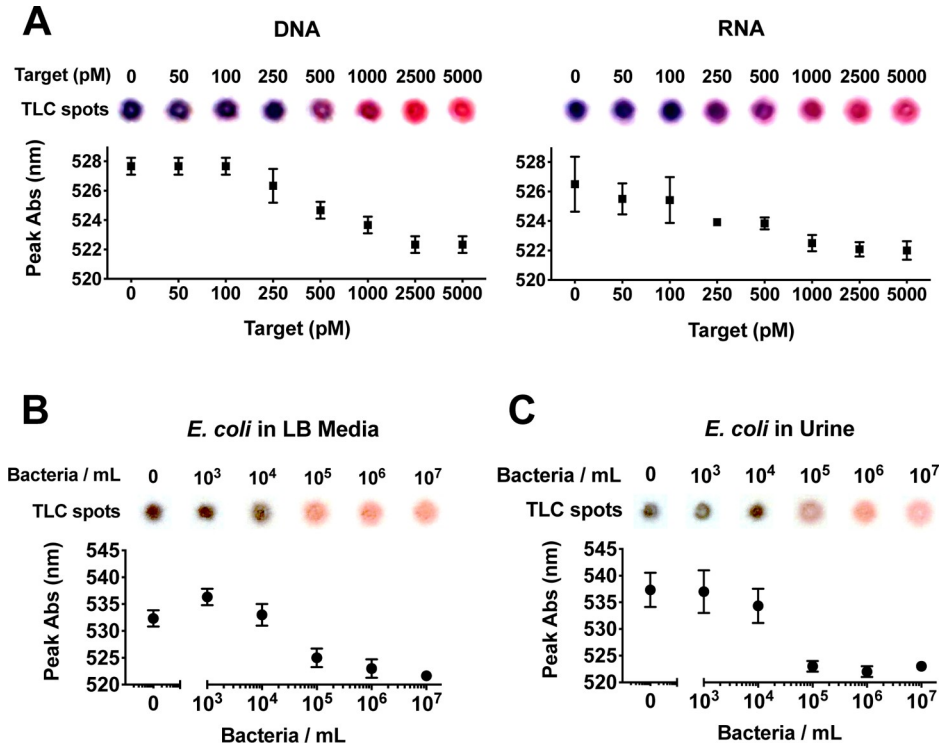

Figure 2. (A) Comparing the sensitivity of DNA and RNA targets. We used water as the "0" negative control. (B) Detection of bacterial RNA extracted from *E. coli* culture. (C) Detection of *E. coli* RNA extracted from urine. Extraction from nonspiked LB media (*B*) or urine (*C*) was used as "0" negative controls. Results are presented as (i) TLC plate color spots and (ii) wavelength corresponding to the peak of the absorbance spectrum. $n = 3$ and error bars are standard deviations. Mz-*E. coli*-V1 was used in (A) and Mz-*E. coli*-V2 (which generates darker negative spots and a higher shift in SPR peak absorbance, also see Figure S1) was used in (B). Therefore, TLC spot colors should not be directly compared between A and B/C.

with the target arms in the inactive state formed a catalytically active enzyme (Figure 1B). Activated Mz could then bind and cleave the linker strand into two-halves, preventing GNP crosslinking and the red-to-purple color change. A single activated Mz could cleave multiple substrates, producing a signal amplification cascade that could be visualized by eye. We can achieve the highest color contrast between the resuspended and crosslinked GNPs by spotting the solution onto a thin layer chromatography (TLC) plate (Figure 1C).[21] The color change correlated with the peak wavelength shift of the GNP absorbance spectrum. Since Mz activity is sequence-specific, we can detect several pathogens in parallel by using multiple Mz enzymes and activating them by different 16S rRNA nucleotide sequences.

Smartphone Readout System

Variations in the TLC plates and user bias can influence the interpretation of the results by the naked eye. We developed software that could automatically identify positive and negative results based on the visual readout to remove this uncertainty. We also built a simple readout device that consisted of a three-dimensional (3D)-printed chassis with the opening for the TLC plate, battery-powered LEDs for uniform illumination of the plate, and a port into which a conventional smartphone could be inserted (Figure 1D). Once the smartphone camera images the plate, the device can automatically upload it to a server. We can process the image to quantify the spots and store the results as a reference for databasing or future analysis. This device provides a simple-to-use platform that ensures objective diagnostic quantification and wireless transmission of test results.

Detecting *E. coli*

To adapt the Mz-GNP assay to detect UTIs, we chose to identify bacterial pathogens based on their 16S rRNA signature. We adopted 10^5 cfu/mL as the positive detection cutoff to match the criterion used for clinical diagnosis.[22] We expect each bacterium to have 10^4 to 10^5 copies of 16S rRNA,[23] yielding 10^9 to 10^{10} 16S rRNA copies/mL, which is within the detection limit of our system.[13] We assessed the detection of RNA using Mz-*E. coli*-V1, which was designed to target the 16S rRNA region of *E. coli* previously used for qPCR analysis.[24] Results confirmed similar detection sensitivities for synthetic DNA and RNA targets (Figure 2A).

We determined the limits of detection of our system. In culture media or spiked into healthy urine, serial dilutions of *E. coli* from 10^3 to 10^7 cfu/mL were tested using alternative Mz-*E. coli*-V2 that produced more pronounced aggregation spots and showed improved sensitivity (Figure S1). Results confirmed *E. coli* detection down to 10^5 cfu/mL (Figure 2B, C). Control experiments included nonspecific Mz (ns-Mz-*E. coli*-V2), Mz inactivated by a key nucleotide mutation (*in1*-Mz-*E. coli*-V2,[25]), or Mz inactivated by scrambling of the catalytic core (in2-Mz-*E. coli*-V2). These targets did not show a positive signal at a high bacterial concentration (10^7 cfu/mL), confirming the observed color change from specific Mz activation by the target (Figure S2). We also demonstrated that an increase in the sample volume to 5 mL led to a decrease in the assay's detection limit of 10^4 cfu/mL (Figure S3). This modification is feasible because urine samples can be up to 50 mL in volume. Thus, one can adjust the detection limit if a lower positive detection cutoff is required.[1]

https://doi.org/10.1021/acsnanoscienceau.2c00001
ACS Nanosci. Au 2022, 2, 324−332

From the perspective of point-of-care assay development, RNA extraction columns might be suboptimal since they require a large bulky centrifuge to achieve the high centrifugation speeds needed to collect the bacterial cells. Therefore, we explored two alternative RNA extraction methods: RNA extraction by magnetic beads and a direct lysis approach. In the lysis approach, lysozyme and proteinase K enzymes release the RNA from the bacterial cells. We directly add the sample to the Mz-GNP system for detection without further purification. The detection limit is 10^5 cfu/mL for both extraction methods (Figure S4). However, we used the well-established spin column-based RNA extraction method for the remainder of this study.

Developing the UTI Pathogen Detection Panel

After validating our experimental scheme with *E. coli*, we expanded the assay to include a panel of the five most common UTI pathogens: *E. coli*, *S. saprophyticus*, *K. pneumoniae*, *P. mirabilis*, and *E. faecalis*. We also introduced a universal bacterial probe (UBP), Mz, which targets a highly conserved region of 16S rRNA and detects all bacteria. It served as a positive control for bacteria-specific Mzs and detected other bacterial pathogens that had no specific Mzs included in the assay. More information on Mz design and optimization is presented in the Supplementary Discussion S1 section and Figures S5 and S6 in the Supporting Information. We found that bacteria-specific conserved regions targeted by these Mzs did not activate all of the probes and the less conserved region targeted by Mz-*E. coli*-V2, so the sample volume had to be increased to 5 mL of cultured bacteria to maintain the required detection sensitivity. All Mzs successfully detected their target bacteria at 10^5 cfu/mL, and all bacterial species activated the UBP (Figure 3 and S7).

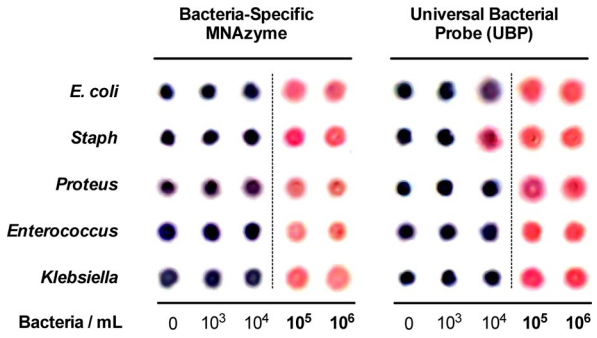

Figure 3. Confirming the sensitivity of the bacteria-specific and UBP Mzs. Dashed line indicates the clinically relevant detection sensitivity of 10^5 cfu/mL. Water was used in place of extracted RNA for the "0" negative control. TLC plate photographs were automatically processed to enhance the color contrast.

To finalize the UTI panel development, we demonstrated the parallel detection of multiple bacterial targets. Six Mz and linker DNA sets were designed and combined into a parallel test mixture to detect a specific UTI pathogen or any bacterium (UBP). We added RNA extracted from one of the cultured bacteria to this solution. Following Mz activation and cleavage, the test mixture was aliquoted into six tubes, each containing one of the target-specific or UBP GNP probes. We successfully detected each bacterial species at 10^5 cfu/mL (Figure 4A). Each target bacterium activated its respective probe. In all cases, UBP reported positive detection (Figure 4B). To confirm the ability of the UBP probe to detect bacteria

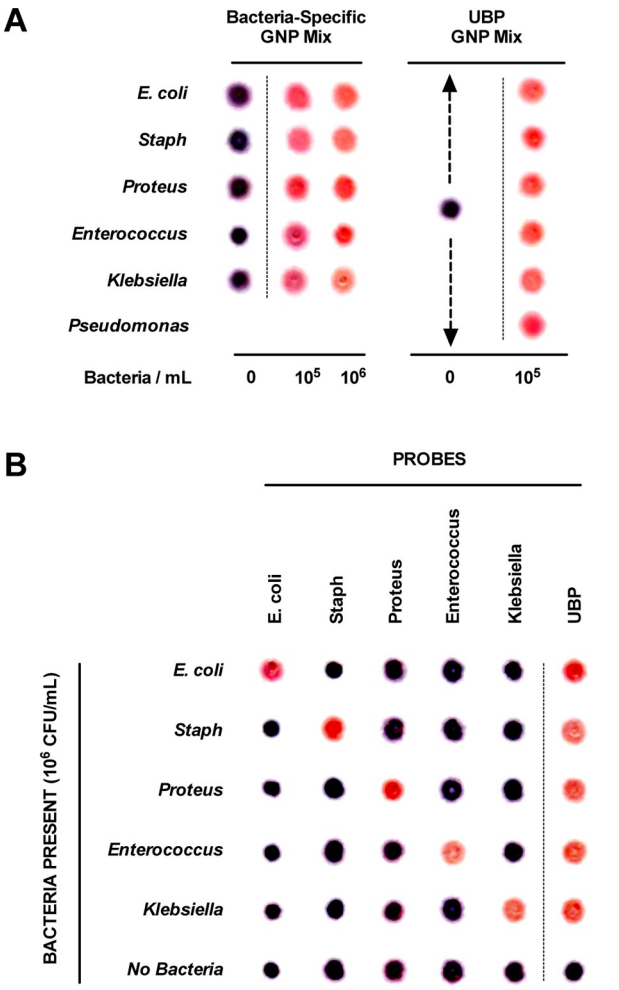

Figure 4. (A) Confirming the sensitivity of the bacteria-specific and UBP Mzs in a parallel detection assay format. The UBP probe can detect *Pseudomonas* bacteria for which no specific Mz was included. (B) Specificity of UTI panel Mzs. Extracted RNA corresponding to 10^6 cultured cfu/mL was used for the experiment. No cross-reactivity between different Mzs is observed. 5 mL of bacterial culture was used for RNA extraction. Water was used in place of extracted RNA for the "0" negative control. TLC plate photographs were automatically processed to enhance the color contrast.

that were not explicitly targeted by any of the Mzs, we included RNA extracted from *P. aeruginosa*. UBP Mz successfully detected this bacterial infection.

Clinical Evaluation

We next evaluated the Mz-GNP assay to probe urine samples from patients with UTI due to *E. coli* (N = 75), *P. mirabilis* (N = 11), and *K. pneumoniae* (N = 34). All positive samples contained bacteria at 10^5 cfu/mL or higher, determined using a standard plating technique performed in the collaborating clinical laboratory in Mount Sinai Hospital, Toronto, Canada. We included the urine of 14 uninfected individuals as negative controls. We also assayed five *E. coli* samples with 10^4 cfu/mL or below. The experiments were carried out in a single-blind format using our smartphone system to automatically identify samples as positive or negative. Figures S8–S12 show the assay results, and Table 1 summarizes the clinical data. We reported negative results for all five *E. coli* samples with bacterial concentrations below 10^5 cfu/mL. Furthermore, we observed only two false-positive results among all Mzs tested. These

https://doi.org/10.1021/acsnanoscienceau.2c00001
ACS Nanosci. Au 2022, 2, 324–332

Table 1. Summary of GNP-Mz UTI Panel Clinical Results for Samples from Patients with *E. coli*, *Proteus*, and *Klebsiella* Infections

Mz target	*E. coli*	*Proteus*	*Klebsiella*	*UBP*
# of infected samples	70	11	34	115
# negative samples[a]	64	123	100	19
true positives	36	7	22	84
true negatives	63	122	100	19
false positives	1	1	0	0
false negatives	34	4	12	31
clinical sensitivity[b]	***51.4%***	***63.6%***	***64.7%***	***73.0%***
clinical Specificity[c]	***98.4%***	***99.2%***	***100%***	***100%***

[a]Negative samples for each pathogen include uninfected controls, samples with subclinical concentrations ($\leq 10^4$ cfu/mL), and samples with infections that are not targeted by the given Mz (e.g., the *Proteus*-positive sample is expected to provide a dark-colored spot for *E. coli* and *Klebsiella* and therefore is included as a negative sample when calculating true negatives for these bacteria). [b]Clinical Sensitivity is calculated as **True Positives** divided by **# of Infected Samples**. [c]Clinical Specificity is calculated as **True Negatives** divided by **# Negative Samples**.

results indicate a clinical specificity of >98.4% for all pathogen-specific and UBP Mz probes. By comparison, clinical sensitivity results were lower: 51.4%, 63.6%, 64.7%, and 73.0%, respectively, for *E. coli*, *Proteus*, *Klebsiella*, and UBP probes. The variable 16S rRNA bacterial expression caused by the interactions of the bacteria with the host environment and immune system could reduce the target concentration in our molecular assay. As a result, this concentration could be below the detection limit, leading to low clinical sensitivity. This type of interaction does not occur in culture experiments. Improving the assay detection limit could be addressed by adding an amplification step in the assay; however, this would add an extra step in the assay. A second approach is to increase the urine collection volume (e.g., up to 50 mL) to reduce the number of false negatives and improve the platform sensitivity. A third approach is to improve the catalytic activity of the Mz.

Table 2 compares the different features of our system to other UTI diagnostic assay formats. The obtained clinical specificity of 98.4% is one of the highest achieved by any UTI tests. Clinical sensitivity numbers between 51.4 and 73.0% are below those obtained using slow bacterial culturing and complex microscopy but are better than those obtained from medical history and physical observation results and are at the medium-to-upper range of the distributions characteristic of urinalysis dipsticks. The execution time of 3 h is at least 6−8 times faster than bacterial culturing assays. While medical history, physical examination, dipstick urinalysis, and microscopy tests are faster to execute, they only provide an indirect indication of the infection and generally cannot identify the pathogen. Therefore, they offer limited diagnostic information. In addition, microscopic observations are labor-intensive, can only test one sample at a time, and require relatively complex equipment, making them unsuitable for point-of-care testing. Our system provides an alternative to current clinical UTI detection methods that can maximize the specificity of the detection, identify the pathogen, and reduce the time for the diagnostic results to be available to the physician.

Cost Analysis

Finally, we estimated the manufacturing cost of our smartphone platform imaging device and per reaction reagent costs. Table S3 presents a breakdown of the cost. Since we designed our device to connect to and use the complex optics, image processing, and wireless transmission capabilities already present in a smartphone, the device can be generated from 3D printing and other low-cost components, yielding a total manufacturing price of only $32.32. The cost of silica column RNA extraction using commercial kits ranges from $1.26 (Biobasic) to $4.10 (ThermoFisher) per sample. However, we can reduce the cost to $0.22 per sample by replacing the commercial kit with third-party silica columns supplemented with in-house-made buffers (Figures S13 and S14 compare extraction efficiencies of commercial kits with third-party columns and in-house buffers). The cost of all Mz-GNP assay components to carry out a six-target UTI panel detection is $0.16 per reaction. Our assay costs $0.38 per sample using a low-cost imaging device connected to a conventional smartphone for sample processing and UTI detection.

DISCUSSION

UTIs affect a significant proportion of the developed and developing world population. This study adapted our colorimetric platform to detect bacterial pathogens in urine samples. The system is simple and cost-effective and does not require expensive equipment, making it adaptable to centralized and remote test locations. It includes a simple optional readout device that combines a conventional smartphone with custom software to quantify assay results. This device reduces user bias, which can affect test outcomes.

Table 2. Comparison of UTI Diagnostic Assays[a]

assay type	clinical sensitivity (%)	clinical specificity (%)	assay time	identify pathogen	major limitations
culturing	100[b]	100[b]	24−48 h	yes	too slow
medical history	11−50	52−92	15 min	no	low sensitivity; limited
physical examination	6−41	79−86	15 min	no	limited information; sensitivity and specificity
urinalysis dipsticks	9−100[c]	19−100[c]	15 min	no	limited information; low sensitivity or specificity
microscopy	78−99	17−63	30 min	limited	limited information ; low specificity; labor- and equipment-intensive
Mz-GNP system (*this study*)	51.4−73.0%	98.4−100%	3 h	yes	limited sensitivity ; slower than dipstick, history, or physical examination

[a]Data from refs 1, 27, and 28. Clinical sensitivity and specificity represent ranges over multiple studies assessed in these references. Only data from studies that considered a positive detection cutoff of $\geq 10^5$ cfu/mL were included to match the inclusion criteria of the current work. [b]Culturing is used to quantify the clinical sensitivity of other methods, assumed to be 100%. [c]The wide distribution of sensitivity and specificity measurements is due to different types of tests used and various selection criteria employed in various studies. In general, urinalysis tests with higher sensitivity lack specificity and those with high specificity have low sensitivity.

https://doi.org/10.1021/acsnanoscienceau.2c00001
ACS Nanosci. Au 2022, 2, 324−332

The smartphone also serves as a transmission device that can wirelessly communicate the test data to a remote server. In the future, this functionality can integrate with a broader network, with the remote devices serving as diagnostic nodes that send the information to a central analytical station. Combining data from multiple nodes can enhance the tracking of the geographic spread of infections. This result, combined with our previous studies on antimicrobial resistance,[14] sets the framework to guide therapeutic decision making in the clinical setting using a simple nanoparticle diagnostic assay system. We expect that these technologies will improve patient outcomes by allowing enhanced antibiotic prescribing practices and proper treatment.

METHODS

Reagents

Sodium citrate monobasic, sodium phosphate dibasic, sodium phosphate tribasic, magnesium chloride, potassium chloride, and $HAuCl_4$ were purchased from Sigma-Aldrich. Tris, Tween-20, and sodium chloride were purchased from BioShop (Burlington, ON, Canada). Hydrochloric and nitric acids were purchased from Caledon Laboratories (Georgetown, ON, Canada). Thiolated methoxyl-terminated polyethylene glycol (PEG) with MW = 1000 Da ($mPEG\text{-}SH_{1000}$) was purchased from Laysan BIO (Arab, AL). Reversed-phase hydrocarbon-impregnated silica gel TLC plates were purchased from Analtech (Newark, DE). All RNA-containing linker DNA strands were acquired from Integrated DNA Technologies (IDT) as a high-performance liquid chromatography (HPLC)-purified lyophilized solid. All other DNA sequences were purchased from BioBasic (Markham, ON, Canada), purified using HPLC (thiol-functionalized sequences) or polyacrylamide gel electrophoresis (nonfunctionalized DNA), and lyophilized by the company. Nanopure distilled water was used for all experiments. DNA sequences used in the study are outlined in Table S1.

Instrumentation

Spectroscopic measurements were performed using a SHIMADZU UV−visible spectrophotometer UV-1601PC (Kyoto, Japan). DLS measurements were performed on a MALVERN Nano-ZS zetasizer (Worcestershire, UK).

Preparation of 13 nm GNPs

98 mL of water and 1 mL of 25 nM $HAuCl_4$ were added to a 250 mL flask prewashed with 40 mL of aqua regia (30 mL HCl, 10 mL nitric acid). The solution was brought to a rapid boil on a benchtop stirring plate (set to 300 °C), and 1 mL of 33 mg/mL sodium citrate tribasic solution was quickly injected under vigorous stirring.[25] The solution was left stirring on the heated plate for 10 min (turning red at around 3 min) and then cooled on ice. DLS measurement was used to confirm the nanoparticle size and monodispersity (polydispersity index of < 0.1 was accepted). Tween-20 was then added to a final concentration of 0.01% (v/v), and nanoparticles were concentrated via 1× centrifugation at 12 000*g* for 30 min. UV−vis spectroscopy was used to determine the nanoparticle concentration by measuring the absorbance at λ = 520 nm (extinction coefficient: $2.33 \times 10^8\ M^{-1}\ cm^{-1}$) and then adjusted to 100 nM using water with 0.01% (v/v) Tween-20.

Adsorbing Thiolated DNA onto GNPs

We followed a slightly modified pH-assisted protocol described previously.[26] 100 μL of 100 nM GNPs were mixed with 100 μL of DNA-L or DNA-R, 40 μL of 0.1% (v/v) Tween-20, and 60 μL of water. All of the DNA-L sequences were added at 2.5 μM concentration (corresponds to a grafting ratio of 25 DNA/GNP), and all of the DNA-R sequences were added at 5 μM concentration (50 DNA/GNP). After 5 min incubation at room temperature (r.t.), 100 μL of 100 mM trisodium citrate (pH 3) buffer was added, and the mixture was incubated for another 30 min at r.t. to allow DNA to adsorb onto GNPs to form GNP-L and GNP-R. 50 μL of 2 mM $mPEG\text{-}SH_{1000}$ was then added, and the solution was incubated for 30 min at 60 °C to stabilize GNPs by backfilling their surface with PEG. Particles were washed via 3× centrifugation at 16 000*g* for 35 min and resuspended in 0.01% (v/v) Tween-20 solution, and their concentration was adjusted to 11 nM.

Standard Single-Target Mz Assay Format

Each reaction was set up by combining 1 μL of 10× Mz buffer (0.1 M Tris−HCl, 0.5 M KCl, pH 8.3), 1 μL of 300 mM $MgCl_2$, 1 μL of appropriate Mz (parts L and R, each at 4 μM), 1 μL of 1 μM Linker, and 6 μL of the test sample in 0.6 mL centrifuge tubes. Test samples could be synthetic DNA or RNA targets (all synthetic target amounts are listed in figures as final concentrations in a 20 μL reaction volume), RNA extracted from bacterial preparation, RNA spiked into healthy urine, or clinical samples. Negative controls used for each experiment are indicated in each figure. A premix for at least five reactions was set up to avoid pipetting small volumes. The tubes were incubated for 1 h 15 min in a 50 °C water bath to allow Mz cleavage to occur. The solution was collected at the bottom via short-pulse spin, and 10 μL of the GNP mix (5 μL of 11 nM GNP_L and 5 μL of 11 nM GNP_R) was then added to each tube. Tubes were incubated for 20 min in a 50 °C water bath to allow linker to hybridize and crosslink GNPs. 3 μL of each sample was spotted on TLC plates. For the experiments that included absorbance measurement, 100 μL of aggregation solution [5 μL of 10× Mz buffer, 5 μL of 300 mM $MgCl_2$, 40 μL of water, and 50 μL of 0.01% (v/v) Tween-20] was added to the remaining 7 μL of the sample, and the absorbance spectrum was measured from 450 to 900 nm.

Multi-Target UTI Panel Mz Assay Format

The reactions were carried out similarly to the standard single-target format with modifications. A single Mz was replaced with a mix of six Mzs, corresponding to one of the bacterial targets or the UBP (4 μM of each of the L and R parts of Mz-*E. coli*, Mz-*Prot*, Mz-*Faec*, Mz-*Staph*, Mz-*Kleb*, and Mz-*UBP*; see Table S1). Similarly, a single linker DNA was replaced with a linker mix consisting of six different linkers: 700 nM Linker-*E. coli*, 900 nM Linker-*Prot*, 700 nM Linker-*Faec*, 900 nM Linker-*Staph*, 800 nM Linker-*Kleb*, and 900 nM Linker-*UBP*. The reaction was set up by mixing 3.5 μL of 10× Mz buffer, 3.5 μL of 300 mM $MgCl_2$, 3.5 μL of 4 μM Mz mix, 3.5 μL of linker mix, and 21 μL of the test sample (RNA extracted from bacteria, clinical samples, or water as the control) in a 1.5 mL Eppendorf tube. The tube was incubated for 1 h 15 min in a 50 °C water bath (for clinical samples, the incubation was extended to 2 h), and then, 5 μL of the solution was transferred into six different 0.5 mL centrifuge tubes, each containing 5 μL of the target-specific GNP mix. For example, one of these tubes would have 2.5 μL of GNP_L-*Prot* and 2.5 μL of GNP_R-*Prot*, while another would contain 2.5 μL of GNP_L-*UBP* and 2.5 μL of GNP_R-*UBP* (See Table S1 for the complete list). The six tubes were then incubated for 20 min in a 50 °C water bath, and 3 μL of the solution was spotted on a TLC plate.

Bacterial Culturing

Cultures of *K. pneumoniae* (HΦ142357), *E. faecalis*, *P. mirabilis*, *S. saprophyticus* (G1101321), and *E. coli* (BW25113) were grown in lysogeny broth (LB) overnight at 37 °C. The samples were then sub-cultured in 5 mL of LB and grown with shaking at 37 °C until the cell density reached 1×10^7 cfu/mL (bacterial concentrations were obtained from standard growth curves generated by culturing serial dilutions of bacteria on LB plates). The cells from the whole culture or 1 mL of the culture were collected by centrifugation at 4500*g* for 5 min at 4 °C. The supernatant was discarded, and RNA was isolated from the bacterial cell pellet using the methods described below.

Detection of Bacteria in Healthy Urine

Bacteria were spiked into urine from healthy noninfected individuals at 10^3, 10^4, 10^5, or 10^6 cfu/mL. 1 mL or 5 mL of the spiked urine was used for RNA extraction.

https://doi.org/10.1021/acsnanoscienceau.2c00001
ACS Nanosci. Au 2022, 2, 324−332

Clinical Sample Collection and Culturing

Urine samples were obtained from the microbiology laboratory at Mount Sinai Hospital (Toronto, Canada) after completing routine clinical cultures. All samples were fully anonymized (only the information on the infecting pathogen provided) and obtained from randomly selected patients (no specific selection criteria applied). Samples were collected in BD gray-capped urine culture tubes containing buffered boric acid (~3.5 mL volume, BD-Canada, Ontario, Canada). Culturing was first carried out by plating 0.001 mL of urine onto Blood Agar and MacConkey Agar and incubating in O_2 at 35 °C for 18−24 h. Growth of up to two potential uropathogens in significant amounts (10^5 cfu/mL) was identified using MS Vitek (bioMerieux Diagnostics, Canada). The growth of three or more different organisms was discarded and reported as no significant growth. The remaining urine was centrifuged for 10 min at 3000*g*, the supernatant was removed, and the pellet was transferred to a 1.5 mL Eppendorf tube. The tube was then filled to the top with TE buffer, briefly vortexed to break the pellet, and centrifuged at 10 000*g* for 1 min. The supernatant was removed, and the TE buffer addition, vortexing, and centrifugation were repeated. After the second centrifugation, the round supernatant was removed, and the pellet was resuspended in a small volume (~50 μL) of TE buffer by vortexing and then frozen and stored at −20 °C before being used for RNA extraction.

RNA Extraction

(i) Spin columns. The volumes of bacterial cultures used for the RNA extraction in each experiment are indicated in the figure captions. For a 1 mL volume, the bacterial culture or urine spiked with bacteria was centrifuged in Eppendorf 1.5 mL tubes at 12 000*g* for 2 min at r.t., the supernatant was removed, and the pellet was resuspended in 100 μL of TE buffer supplemented with 3 mg/mL lysozyme. For a 5 mL volume, the sample was first divided into three 1.5 mL tubes and then centrifuged at 12 000*g* for 2 min, and the pellet was combined and resuspended in 100 μL of lysozyme-supplemented TE buffer. The samples were incubated for 7 min at room temperature to lyse the bacterial cell wall. RNA from cultured or urine-spiked bacteria was then extracted using a Bio Basic EZ-10 Spin Column Total RNA Mini-Preps Super Kit (Markham, Canada). The standard manufacturer's protocol was followed. RNA from clinical samples was extracted using a GeneJET RNA purification kit (ThermoFisher) following the manufacturer protocol. *(ii) Magnetic Kit.* 1 mL of the bacterial culture was centrifuged at 12 000*g* for 2 min at r.t., the supernatant was removed, and the standard protocol from the MagJET RNA purification kit (ThermoFisher) was followed with a 0.4 mg/mL (final) lysozyme 7 min incubation step. 100 μL of water was used for the final elution step. *(iii) Direct lysis.* 1 mL of the bacterial culture was centrifuged at 6000*g* for 5 min at r.t., and the supernatant was discarded down to ~ 20 μL. 50 μL of 800 μg/mL lysozyme, 2 μL of 20 mg/mL proteinase K, and 7 μL of 10× Mz buffer were added and incubated at 37 °C for 1 h. The solution was centrifuged at 6000*g* for 5 min to settle the cellular residue. 6 μL of the supernatant was used directly for the Mz assay.

Smartphone Plate Readout Device

A case specific to the Google Nexus 5 smartphone was designed using CAD software and 3D-printed using polylactic acid filament on a MakerBot Replicator 2 3D printer. The case included an opening for the insertion of a TLC plate. The imaging distance between the smartphone camera and the plate was 80 mm. Indirect diffuse illumination was achieved using four LEDWE-15 white LEDs obtained from Thorlabs reflected against the wall of the case onto the substrate to be imaged. The device was powered by a 9 V battery integrated into the case.

Plate Processing Using Image J Software

All images of spots used in figures were processed in Image J software with 3 × 3 pixel neighborhood median filtering and 50-pixel rolling ball background subtraction applied to each color channel individually. The filtered monochrome images were combined into a processed color image, followed by manual histogram stretching. The macro source code is provided in the supplementary file named "CleanupMacro.ijm".

Spot Quantification Using Matlab Software

A partially automated process flow was implemented in Matlab for labeling each spot with the median red signal of its pixels (source code provided in the supplementary file named "labeller_red.m"). Image processing consisted of 3 × 3 pixel neighborhood median filtering, 100 × 100 neighborhood top-hat filtering, and contrast adjustment. Then, the image is displayed, allowing the user to specify the region of the image containing spots and the positive and negative control spots in the image. Then, spots are defined as connected components from the Otsu threshold of the sum of the blue and green channels of the preprocessed image. The median red values of the pixels within the spot are measured for each spot. The exact color of both positive and negative spots can be affected by such factors as specific Mz molecules used and small variation between TLC plates. To account for these variations, the median red signals for the spots on each TLC plate are normalized to values between 0 and 100, with the negative spot being assigned a value of 0 and the positive red spot assigned a value of 100. The script then exports a processed image file with each of the measured median red values listed beside each spot (on the right). Any spot that has a normalized red signal value of 36 to 100 is identified as positive and any spot with the red value of 0 to 35 as negative. These numbers were then collated across all images. One potential limitation of this analysis is that the cutoff value of 35 was chosen manually based on the analysis of multiple TLC plates. The criteria were to ensure that the spots that we consider negative with our trained eyes would also be recorded as negative by the software algorithm. This approach could potentially introduce a systematic error into the automated analysis of experimental results: some mildly red spots that could potentially be weakly positives would be recorded as negative by the software. To estimate the defect of this systematic error, we changed the cutoff value from 35 to 40 and reran patient sample analysis. We found that the readout of only 4 out of 536 total spots was affected, indicating a limited effect of this potential systematic error.

Study Approval

Ethics exemption was provided as these were residual urine specimens that were anonymized entirely (except for the culture results) and would typically be discarded once routine culture was completed.

■ ASSOCIATED CONTENT

Supporting Information

The Supporting Information is available free of charge at https://pubs.acs.org/doi/10.1021/acsnanoscienceau.2c00001.

Nucleic acid sequences used in this study, cost estimates of the device, additional pathogen diagnostic data, extraction and assay characterization data, and complete methods and procedures (PDF)

■ AUTHOR INFORMATION

Corresponding Author

Warren C.W. Chan − *Institute of Biomedical Engineering, University of Toronto, Toronto, Ontario M5S 3G9, Canada; Donnelly Centre for Cellular and Biomolecular Research, University of Toronto, Toronto, Ontario M5S 3E1, Canada;* orcid.org/0000-0001-5435-4785; Email: warren.chan@utoronto.ca

Authors

Kyryl Zagorovsky − *Institute of Biomedical Engineering, University of Toronto, Toronto, Ontario M5S 3G9, Canada; Donnelly Centre for Cellular and Biomolecular Research, University of Toronto, Toronto, Ontario M5S 3E1, Canada*

https://doi.org/10.1021/acsnanoscienceau.2c00001
ACS Nanosci. Au 2022, 2, 324−332

Maria Teresa Fernández-Argüelles − *Institute of Biomedical Engineering, University of Toronto, Toronto, Ontario M5S 3G9, Canada; Donnelly Centre for Cellular and Biomolecular Research, University of Toronto, Toronto, Ontario M5S 3E1, Canada; Department of Physical and Analytical Chemistry, University of Oviedo, Oviedo, Asturias 33006, Spain*

Diane Bona − *Department of Biochemistry, University of Toronto, Toronto, Ontario M5G 1M1, Canada*

Ashraf Mohamed Elshawadfy − *Donnelly Centre for Cellular and Biomolecular Research, University of Toronto, Toronto, Ontario M5S 3E1, Canada; Department of Botany and Microbiology, Zagazig University, Zagazig 44519, Egypt*

Abdullah Muhammad Syed − *Institute of Biomedical Engineering, University of Toronto, Toronto, Ontario M5S 3G9, Canada; Donnelly Centre for Cellular and Biomolecular Research, University of Toronto, Toronto, Ontario M5S 3E1, Canada; Gladstone Institute of Data Science and Biotechnology, San Francisco, California 94158, United States;* orcid.org/0000-0001-9156-9662

Pranav Kadhiresan − *Institute of Biomedical Engineering, University of Toronto, Toronto, Ontario M5S 3G9, Canada; Donnelly Centre for Cellular and Biomolecular Research, University of Toronto, Toronto, Ontario M5S 3E1, Canada*

Tony Mazzulli − *Department of Microbiology, Mount Sinai Hospital/University Health Network, Toronto, Ontario M5G 1X5, Canada*

Karen L. Maxwell − *Department of Biochemistry, University of Toronto, Toronto, Ontario M5G 1M1, Canada*

Complete contact information is available at: https://pubs.acs.org/10.1021/acsnanoscienceau.2c00001

Author Contributions

[▽]K.Z. and M.T.F.A. contributed equally to this work.

Author Contributions

K.Z., M.T.F., D.B., T.M., K.L.M., and W.C.W.C. designed the study; K.Z., M.T.F., and A.M.E. performed the Mz-GNP assay development and testing of cultured bacteria and clinical samples; D.B. and K.L.M. carried out bacterial culturing and RNA extraction from cultured bacteria and clinical samples; T.M. and G.M. provided clinical samples; G.M. carried out clinical sample preprocessing; P.K. built the smartphone imaging device prototype; A.S. developed the MatLab and ImageJ algorithms for TLC plate post-image processing and spot color quantification; K.Z., M.T.F., D.B., and W.C.W.C. analyzed the data; and K.Z. and W.C.W.C. wrote the paper.

Notes

The authors declare the following competing financial interest(s): We have a start company called Luna Nanotech that will commercialize this technology.

■ ACKNOWLEDGMENTS

This work was supported by the Natural Sciences and Engineering Research Council of Canada (CHRPJ-523436 and 950-223824) and the Canadian Institute of Health Research (CPG-158270-S). K.Z. and A.M.S. acknowledge a graduate student fellowship from NSERC.

■ REFERENCES

(1) Schmiemann, G.; Kniehl, E.; Gebhardt, K.; Matejczyk, M. M.; Hummers-Pradier, E. The diagnosis of urinary tract infection: a systematic review. *Dtsch Arztebl Int.* **2010**, *107*, 361−367.

(2) Maclennan, C.; Swingler, G.; Craig, J. *Urinary Tract Infections in Infants and Children in Developing Countries in the Context of IMCI*; World Health Organization, 2005.

(3) Ronald, A. The etiology of urinary tract infection: traditional and emerging pathogens. *Dis Mon.* **2003**, *49*, 71−82.

(4) Lee, J. B. L.; Neild, G. H. Urinary tract infection. *Medicine* **2007**, *35*, 423−428.

(5) Sheerin, N. S. Urinary tract infection. *Medicine* **2011**, *39*, 384−389.

(6) Luna, C. M.; et al. Appropriateness and delay to initiate therapy in ventilator-associated pneumonia. *Eur. Respir. J.* **2006**, *27*, 158−164.

(7) Iregui, M.; Ward, S.; Sherman, G.; Fraser, V. J.; Kollef, M. H. Clinical Importance of Delays in the Initiation of Appropriate Antibiotic Treatment for Ventilator-Associated Pneumonia. *Chest* **2002**, *122*, 262−268.

(8) Barenfanger, J.; Drake, C.; Kacich, G. Clinical and Financial Benefits of Rapid Bacterial Identification and Antimicrobial Susceptibility Testing. *J. Clin. Microbiol.* **1999**, *37*, 1415−1418.

(9) Trenholme, G. M.; et al. Clinical impact of rapid identification and susceptibility testing of bacterial blood culture isolates. *J. Clin. Microbiol.* **1989**, *27*, 1342−1345.

(10) Doern, G. V.; Vautour, R.; Gaudet, M.; Levy, B. Clinical impact of rapid in vitro susceptibility testing and bacterial identification. *J. Clin. Microbiol.* **1994**, *32*, 1757−1762.

(11) Hartman, M. R.; et al. Point-of-care nucleic acid detection using nanotechnology. *Nanoscale* **2013**, *5*, 10141.

(12) Zhang, Y.; et al. Surveilling and tracking COVID-19 patients using a portable quantum dot smartphone device. *Nano Lett.* **2021**, *21*, 5209.

(13) Zagorovsky, K.; Chan, W. C. W. A Plasmonic DNAzyme Strategy for Point-of-Care Genetic Detection of Infectious Pathogens. *Angew. Chem. Int. Ed.* **2013**, *52*, 3168−3171.

(14) Abdou Mohamed, M. A.; et al. Diagnosing antibiotic resistance using nucleic acid enzymes and gold nanoparticles. *ACS Nano* **2021**, *15*, 9379−9390.

(15) Kozlowski, H. N.; et al. A Colorimetric Test to Differentiate Patients Infected with Influenza from COVID-19. *Small Struct.* **2021**, *2*, 2100034.

(16) Hurst, S. J.; et al. Maximizing DNA Loading on a Range of Gold Nanoparticle Sizes. *Anal. Chem.* **2006**, *78*, 8313−8318.

(17) Quinten, M.; Kreibig, U.; Schönauer, D.; Genzel, L. Optical absorption spectra of pairs of small metal particles. *Surf. Sci.* **1985**, *156*, 741−750.

(18) Schlosser, K.; Li, Y. A Versatile Endoribonuclease Mimic Made of DNA: Characteristics and Applications of the 8-17 RNA-Cleaving DNAzyme. *ChemBioChem* **2010**, *11*, 866−879.

(19) Santoro, S. W.; Joyce, G. F. A general purpose RNA-cleaving DNA enzyme. *Proc. Natl. Acad. Sci. U.S.A.* **1997**, *94*, 4262−4266.

(20) Mokany, E.; Bone, S. M.; Young, P. E.; Doan, T. B.; Todd, A. V. MNAzymes, a Versatile New Class of Nucleic Acid Enzymes That Can Function as Biosensors and Molecular Switches. *J. Am. Chem. Soc.* **2010**, *132*, 1051−1059.

(21) Elghanian, R.; Storhoff, J. J.; Mucic, R. C.; Letsinger, R. L.; Mirkin, C. A. Selective colorimetric detection of polynucleotides based on the distance-dependent optical properties of gold nanoparticles. *Science* **1997**, *277*, 1078−1081.

(22) Kwon, J. H.; Fausone, M. K.; Du, H.; Robicsek, A.; Peterson, L. R. Impact of laboratory-reported urine culture colony counts on the diagnosis and treatment of urinary tract infection for hospitalized patients. *Am. J. Clin. Pathol.* **2012**, *137*, 778−784.

(23) Zwirglmaier, K.; Ludwig, W.; Schleifer, K.-H. Recognition of individual genes in a single bacterial cell by fluorescence in situ hybridization - RING-FISH. *Mol. Microbiol.* **2003**, *51*, 89−96.

(24) Chung, H. J.; Castro, C. M.; Im, H.; Lee, H.; Weissleder, R. A magneto-DNA nanoparticle system for rapid detection and phenotyping of bacteria. *Nat. Nanotechnol.* **2013**, *8*, 369−375.
(25) Perrault, S. D.; Walkey, C.; Jennings, T.; Fischer, H. C.; Chan, W. C. W. Mediating Tumor Targeting Efficiency of Nanoparticles Through Design. *Nano Lett.* **2009**, *9*, 1909−1915.
(26) Zhang, X.; Servos, M. R.; Liu, J. Instantaneous and Quantitative Functionalization of Gold Nanoparticles with Thiolated DNA Using a pH-Assisted and Surfactant-Free Route. *J. Am. Chem. Soc.* **2012**, *134*, 7266−7269.
(27) Meister, L.; Morley, E. J.; Scheer, D.; Sinert, R. History and Physical Examination Plus Laboratory Testing for the Diagnosis of Adult Female Urinary Tract Infection. *Acad. Emerg. Med.* **2013**, *20*, 631−645.
(28) Wilson, M. L.; Gaido, L. Laboratory diagnosis of urinary tract infections in adult patients. *Clin. Infect. Dis.* **2004**, *38*, 1150−1158.

https://doi.org/10.1021/acsnanoscienceau.2c00001
ACS Nanosci. Au 2022, 2, 324−332